

# Effect of high-temperature neutron irradiation on fracture toughness of ITER-specification tungsten

C Yin<sup>1,2</sup>, D Terentyev<sup>1</sup>, S Van Dyck<sup>1</sup>, A Stankovskiy<sup>1</sup>, R H Petrov<sup>3,4</sup> and T Pardoen<sup>2</sup>

<sup>1</sup>Structural Materials Group, Institute of Nuclear Materials Science, SCK-CEN, 2400 Mol, Belgium

<sup>2</sup>Institute of Mechanics, Materials and Civil Engineering, UCLouvain, 1348 Louvain-la Neuve, Belgium

<sup>3</sup>Department of Electrical Energy, Metals, Mechanical Constructions & Systems, Ghent University, 9052 Ghent, Belgium

<sup>4</sup>Department of Materials Science and Engineering, Delft University of Technology, Delft, 2082, The Netherlands

E-mail: [cyin@sckcen.be](mailto:cyin@sckcen.be)

Received 26 May 2019, revised 20 September 2019

Accepted for publication 6 November 2019

Published 16 March 2020



CrossMark

## Abstract

The effect of neutron irradiation on the fracture toughness of two commercially pure tungsten materials processed according to ITER specifications has been investigated for three doses: 0.08 dpa, 0.44 dpa, and 0.67 dpa at 600 °C. The choice of this temperature was motivated by its technological importance due to the risk of irradiation-induced embrittlement. The temperature of 600 °C is below the void swelling peak temperature (~800 °C) and, at the same time, well above the ductile to brittle transition temperature (DBTT) of the reference material (~300 °C). Neutron irradiation was performed in the BR2 material test reactor inside the fuel channel in order to limit the transmutation of rhenium and osmium close to the rates expected in a fusion environment. The results of the mechanical tests performed up to 600 °C show that the fracture toughness decreases with the increase in the irradiation dose for both tungsten products. The fracture surfaces of the non- and irradiated specimens were systematically analysed to determine the evolution of the failure mechanisms.

Keywords: tungsten, fracture toughness, neutron irradiation, nuclear fusion, high temperature

(Some figures may appear in colour only in the online journal)

## Introduction

The neutron irradiation effect on the mechanical properties of tungsten is considered to be a key element in the design of the plasma facing components (PFC) for ITER in the nuclear phase operation [1–3]. The divertor PFC will be exposed to a high heat flux load during normal operation, where the temperature from the contact with the heat sink material to the top surface varies from 300 °C to 1200 °C (for power loads of 15 MW m<sup>-2</sup>) [4]. Therefore, a database of mechanical properties that accounts for the combination of the temperature gradient and neutron irradiation is required.

Currently, tungsten is the main candidate material for PFCs, including the divertor of ITER and the first wall armor

in DEMO, where much higher neutron flux compared to ITER is expected. To date, most of the studies on the neutron irradiation effects on the mechanical properties of tungsten have been focused on modeling and measurement of hardness [5–14]. However, the latter was performed at room temperature, which cannot be considered as a representative test condition for PFCs. Only a few studies, performed in the 1970s and after 2016, addressed the changes in the tensile and bending properties of tungsten, which was irradiated by neutrons in fast and mixed spectra reactors, including high-temperature irradiation and testing, namely up to 800 °C [15–17]. To date, no information on the change in the fracture toughness after neutron irradiation is available, while this gap needs to be closed to perform at least a computational

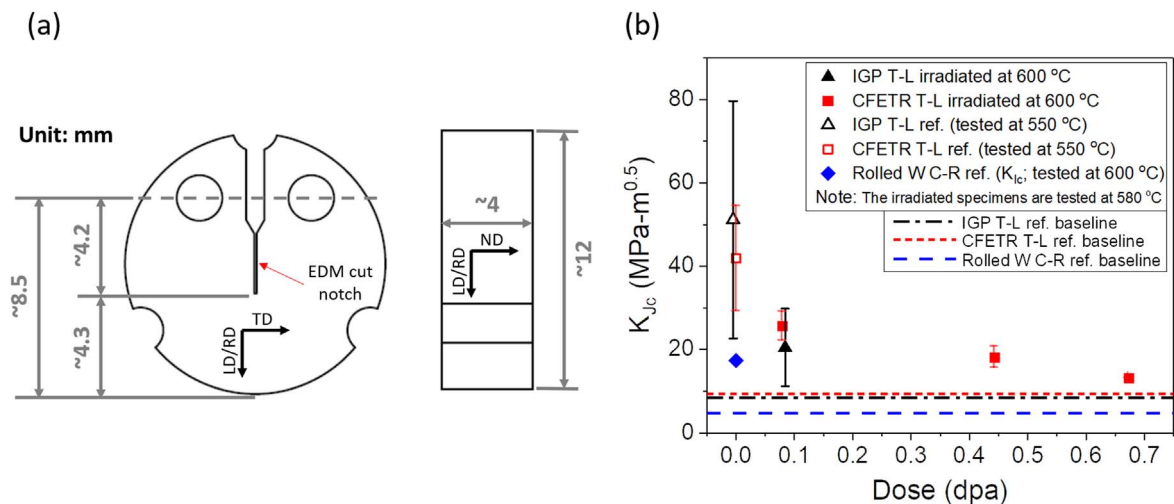


**Figure 1.** (a) A sketch and dimensions of the DCT specimens (TD: transverse direction; ND: normal direction); (b) the  $K_{Jc}$  as a function of the irradiation dose for the IGP T-L and CFETR T-L (the data of the reference specimens is detailed in our previous work [26]); the  $K_{Jc}$  value (only considers linear elastic fracture behavior) of rolled W C-R, which can be considered as the lower limit of the fracture toughness, is referred to in Faleschini *et al* [36]); the baselines are defined as the fracture toughness at room temperature; more than two specimens were tested at each test temperature to obtain minimum statistics; the error bars represent one standard deviation of the experimental data.

assessment of the structural integrity of PFCs in normal and off-normal operating regimes [18].

The aim of this study is to investigate the change in fracture toughness and fracture surface morphology after neutron irradiation at 0.08, 0.44, and 0.67 dpa of two tungsten products fabricated according to ITER specifications [19]. The selected doses for neutron irradiation refer to the accumulated end-of-life dose in ITER PFCs, which is expected to be less than 1 dpa [20]. The irradiation and maximum test temperature has been selected at 600 °C, below the peak swelling [21–23], and yet considerably above the ductile to brittle transition temperature (DBTT) of typical commercial tungsten products [24, 25].

## Methodology

Two ITER-specification tungsten products are considered in this study: European ITER grade tungsten (IGP, manufactured by Plansee, Austria, by double hammering and supplied as a rod) and Chinese ITER grade tungsten (CFETR, manufactured by AT&M, China, by rolling and supplied in the shape of a plate). As a result, the IGP has elongated carrot-like grains aligned in the longitudinal direction (LD), whereas the CFETR has flat pancake-like grains ‘flattened’ along the rolling direction (RD) [26]. The equivalent median diameter of a grain (defined by a high-angle grain boundary with a misorientation angle between grains larger than 15°), measured on the plane perpendicular to the normal direction (ND), is around 100  $\mu\text{m}$  and 70  $\mu\text{m}$  for IGP and CFETR, respectively. Additionally, a sub-grain structure (misorientation angle between 5 to 15°) with a sub-grain size of several  $\mu\text{m}$  was observed in both materials. More detailed information on the microstructure and mechanical properties of these products can be found in our previous work [26].

Disk-shaped compact tension (DCT) specimens were machined with a narrow notch with a root radius around 50–90  $\mu\text{m}$  produced by electrical discharge machining (EDM). The notch machined in the specimens for both materials is parallel to the T-L plane, as imposed in the ASTM E399 standard [27]. A schematic of the specimen’s geometry with dimensions is shown in figure 1(a).

Neutron irradiation was performed in the Belgian Material Test Reactor (BR2) inside the fuel element in the position close to the center of the reactor and in a mid-plane where the fast neutron ( $E > 0.1$  MeV) flux is  $7 \times 10^{14}$  n/cm<sup>2</sup>/s at a power of 60 MW. The samples were encapsulated in a steel tube with 1.5 mm wall thickness filled with He. The gap between the samples and the pressure tube was adjusted to achieve 600 °C during the irradiation following the thermal and neutronic calculations. Following finite element analysis of thermal flow, a variation of about 25 °C could occur due to the burn out of the fuel element within a reactor cycle. The irradiation dose was calculated by MCNPX 2.7.0 [28] and found to be 0.08 dpa, 0.44 dpa, and 0.67 dpa. The dpa cross sections for W have been estimated from the JENDL4 file (MT444) for the threshold displacement energy of 55 eV, following the recommendations of International Atomic Energy Agency (IAEA) [29]. The transmutation of Re and Os is calculated based on the ALEPH code developed by SCK · CEN and available nuclear databases [30–34]. The upper limit of the summed concentration (at%) of Re and Os together is 0.61 at%, 0.97 at%, and 1.40 at% for 0.08 dpa, 0.44 dpa, and 0.67 dpa, respectively. The fraction of Os is about 1% of the total produced Re and Os.

The  $K_{Jc}$  values (elastic–plastic equivalent stress intensity factor) of the irradiated specimens are determined according to the requirements of the ASTM E1921 [35]. The fracture toughness tests for irradiated and non-irradiated specimens are carried out in air using a universal testing machine (INSTRON

3800) with an environmental furnace. The test temperature for the irradiated specimens ranges from 400 °C to 580 °C. To obtain homogeneous temperature distribution and to limit surface oxidation, the heated specimens are exposed to an elevated temperature for only 30 min prior to the start of the test. The test itself lasted for a few minutes or less. The reference measurements were reported in our previous work [26]. The qualitative and quantitative analyses of the microstructures of the fracture surfaces (fraction of fracture type) were carried out by ImageJ analysis software on scanning electron microscopy (SEM) images at appropriate magnifications.

In this paper, we present the results of mechanical tests performed for both products at 0.08 dpa, and higher dose data are shown for CFETR tungsten only. Our preliminary study showed that the fracture toughness of the IGP irradiated to 0.44 dpa requires testing to be performed above 600 °C, which is the upper limit of this study.

## Results and discussion

Figure 1(b) shows the variation in the fracture toughness with irradiation dose, together with the reference values measured at room temperature, i.e. in the brittle, non-irradiated conditions. For both tested products, the measured  $K_{Jc}$  value decreases with the increasing irradiation dose. At the highest dose studied here (0.67 dpa), the  $K_{Jc}$  value of CFETR T-L is reduced almost down to the fracture toughness at room temperature. This indicates that the irradiation to 0.67 dpa has raised the DBTT of this product up to  $\sim 600$  °C, which corresponds to an increase of 300 °C (see [26] for reference measurements). The irradiation-induced changes in the microstructure in the studied samples is currently under investigation. However, as reported in the literature [12], the hardening and subsequent embrittlement induced by neutron irradiation depend not only on the fluence and irradiation temperature but also on the neutron spectrum, which defines the transmutation rate. Transmuted elements (Re and Os) are found to form secondary phases ( $\sigma$  phase and  $\chi$  phase), while displacement damage creates voids and dislocation loops in the temperature and dose range studied here [11, 13]. The presence of precipitates, voids, and dislocation loops decreases the mobility of dislocations causing hardening. As a result, the ductility and capacity to dissipate energy by plastic deformation of irradiated material is reduced such that it loses its fracture toughness, i.e. it becomes brittle. Moreover, the irradiation-induced defects can also act as stress concentration sites, thus affecting the crack propagation not only below and but also above the DBTT region.

The amount by which the  $K_{Jc}$  is reduced by the irradiation is different for the two types of tested materials. IGP T-L exhibits a larger reduction in the  $K_{Jc}$  compared to the CFETR T-L product. In addition, the scatter in the  $K_{Jc}$  value also decreases with the increase in the irradiation dose. This is probably related to the fact that the neutron irradiation-induced defects, homogeneously distributed in the material, also act as stress concentrators reducing the statistical spread of the defects controlling the fracture of the non-irradiated state.

Figure 2 shows a collection of the fracture surface morphologies from which transgranular surface fraction has been determined. The morphology of the fracture patterns of both materials, although tested after different irradiation doses, look quite similar. At a temperature below 550 °C (figures 2(a), (c), (e), (g), (i), and (k)), the fracture surfaces of all specimens, whether they were irradiated or not, exhibit a mixture of intergranular and transgranular brittle fracture. However, intergranular ductile dimples start to appear at the test temperature above 550 °C (figures 2(b), (d), (f), (h), (j), and (l)) for non-irradiated and irradiated specimens. When the test temperature rises up to 600 °C, the intergranular brittle fracture is no longer observed in the non-irradiated materials, as also reported in [26]. The fact that the intergranular brittle fracture mode disappears on the fracture surface of irradiated specimens at the test temperature equal to 600 °C will require further investigation.

The surface ratio of the transgranular brittle fracture mode, calculated by ImageJ analysis of the SEM images, is given in figure 3. For most of the inspected conditions, the fraction of the transgranular brittle fracture is larger in the CFETR product. Moreover, for the CFETR product, the fraction of the transgranular brittle fracture is seen to increase with the increase in the irradiation dose, which is likely related to the suppression of dislocation-mediated plasticity inside the grains caused by the presence of the irradiation-induced defects (dislocation loops, voids, and probably Re/Os precipitates). In the IGP T-L product, the irradiation at 0.08 dpa does not impact the amount of transgranular brittle fracture. This difference between the fracture patterns of the IGP and CFETR materials can be ascribed to the difference in the shape of the grains, and mutual grain-crack orientation in the studied products [26]. The IGP has carrot-like grains along the crack propagation direction, and the CFETR has pancake-like grains perpendicular to the crack propagation plane [26]. As a result, the IGP exhibits a lower propensity for transgranular brittle fracture than the CFETR product [26]. The confirmation of this hypothesis, as well as a physical explanation for the observed embrittlement, requires detailed transmission electron microscopy study as well as the measurement of the chemical composition (i.e. Re and Os) in the irradiated samples, which is currently in progress.

## Conclusions

Based on the results obtained up to now, we can draw the following conclusions:

- (i) The  $K_{Jc}$  measured at 580 °C progressively decreases with the increasing irradiation dose down to  $\sim 10 \text{ MPa} \cdot \sqrt{m}$ , i.e. approaching the room temperature fracture toughness of this material. This indicates that neutron irradiation at 600 °C, which is similar to the condition to be faced by the divertor tungsten monoblock in the region close to the cooling pipe, leads to the shift of the DBTT by 300 °C as the neutron fluence

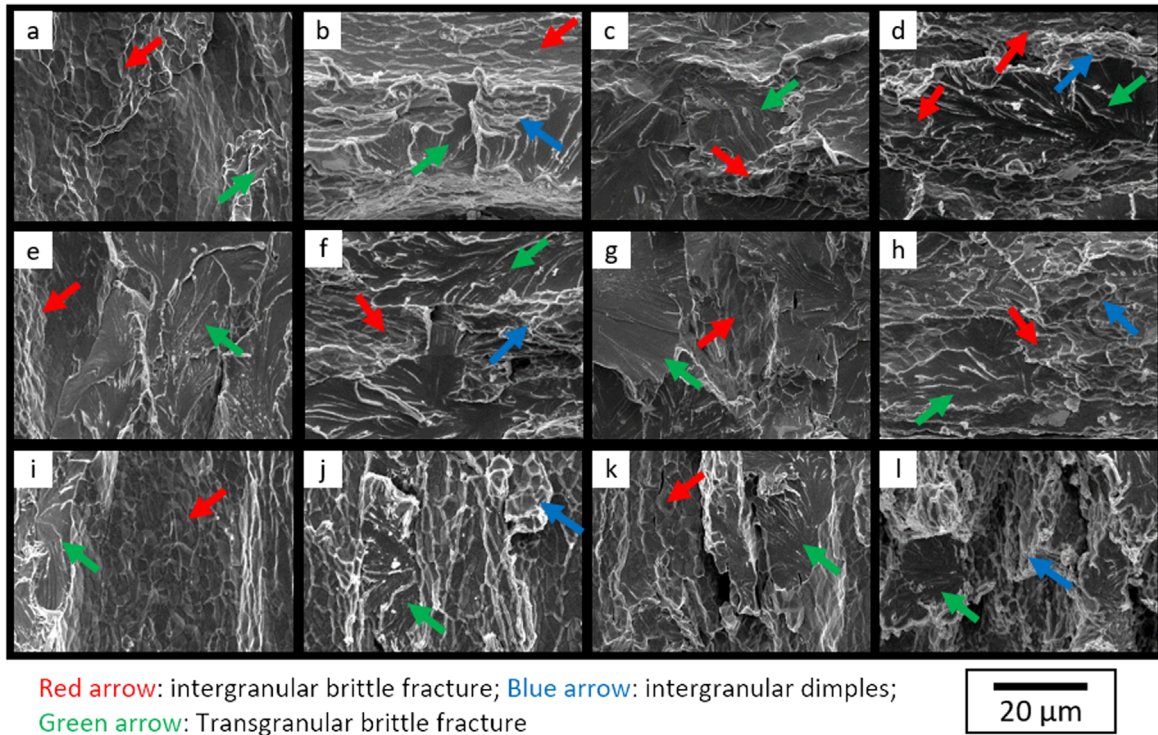


**Figure 2.** Fracture surfaces of the DCT specimens. IGP T-L 0.08 dpa tested at 500 °C (a) and 580 °C (b); CFETR T-L 0.08 dpa tested at 400 °C (c) and 580 °C (d); CFETR T-L 0.44 dpa tested at 500 °C (e) and 580 °C (f); CFETR T-L 0.67 dpa tested at 500 °C (g) and 580 °C (h); IGP T-L reference tested at 500 °C (i) and 600 °C (j); CFETR T-L reference tested at 500 °C (k) and 600 °C (l).

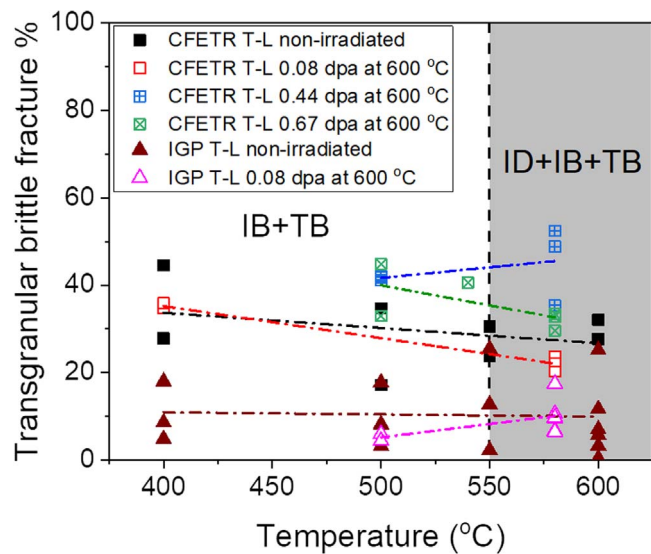


**Figure 3.** Variation of the fraction of transgranular brittle fracture as a function of test temperature: each data point in the plot represents the fraction of fracture feature corresponding to one specimen. IB: intergranular brittle; TB: transgranular brittle; ID: intergranular dimple.

progressively increases, i.e. the irradiation makes the material brittle under the irradiation conditions. Note that the dose of 0.67 dpa is close to the design end-of-life dose for the ITER divertor components. However, the concentration of transmuted elements after

irradiation in BR2 is different (approximately a factor of two higher) from the one expected in the fusion environment due to a higher fraction of thermal-to-fast neutrons. Understanding the impact of enhanced transmutation due to fission environment remains a truly challenging problem for which the most natural solution is the application of a fast fission spectrum (i.e. the use of CEFR or BOR60 reactors).

- (ii) The appearance of dimples on the fracture surface (at  $T_{test} > 550$  °C) seems to be the only clear temperature-dependent microstructural feature observed by SEM in this study.
- (iii) The portion of the transgranular brittle fracture pattern in the CFETR T-L material increases after irradiation, which can be explained by the obstruction of the plastic deformation of grains due to pinning of dislocations at irradiation-induced defects. However, the same trend is not observed in the IGP T-L material.

**Acknowledgments**

This work has been carried out within the framework of the EUROfusion Consortium and has received funding from the Euratom research and training programme 2014–2018 and 2019–2020 under Grant No. 633053. The views and opinions expressed herein do not necessarily reflect those of the European Commission.

## References

- [1] Davis J, Barabash V, Makhankov A, Plöchl L and Slattery K 1998 Assessment of tungsten for use in the ITER plasma facing components *J. Nucl. Mater.* **258** 308–12
- [2] Zinkle S and Ghoniem N 2000 Operating temperature windows for fusion reactor structural materials *Fusion Eng. Des.* **51** 55–71
- [3] Barabash V, Federici G, Rödiger M, Snead L and Wu C 2000 Neutron irradiation effects on plasma facing materials *J. Nucl. Mater.* **283** 138–46
- [4] You J *et al* 2018 European divertor target concepts for DEMO: design rationales and high heat flux performance *Nucl. Mater. Energy.* **16** 1–11
- [5] Huang C-H, Gilbert M R and Marian J 2018 Simulating irradiation hardening in tungsten under fast neutron irradiation including Re production by transmutation *J. Nucl. Mater.* **499** 204–15
- [6] Zhao Q, Zhang Z, Huang M and Ouyang X 2019 Effects of transmutation elements in tungsten *Comput. Mater. Sci.* **162** 133–9
- [7] Hu X *et al* 2016 Irradiation hardening of pure tungsten exposed to neutron irradiation *J. Nucl. Mater.* **480** 235–43
- [8] Hasegawa A, Tanno T, Nogami S and Satou M 2011 Property change mechanism in tungsten under neutron irradiation in various reactors *J. Nucl. Mater.* **417** 491–4
- [9] Hasegawa A, Fukuda M, Tanno T and Nogami S 2013 Neutron irradiation behavior of tungsten *Mater. Trans.* **54** 466–71
- [10] Fukuda M, Hasegawa A, Tanno T, Nogami S and Kurishita H 2013 Property change of advanced tungsten alloys due to neutron irradiation *J. Nucl. Mater.* **442** S273–6
- [11] Hasegawa A, Fukuda M, Nogami S and Yabuuchi K 2014 Neutron irradiation effects on tungsten materials *Fusion Eng. Des.* **89** 1568–72
- [12] Fukuda M *et al* 2016 Neutron energy spectrum influence on irradiation hardening and microstructural development of tungsten *J. Nucl. Mater.* **479** 249–54
- [13] Hasegawa A, Fukuda M, Yabuuchi K and Nogami S 2016 Neutron irradiation effects on the microstructural development of tungsten and tungsten alloys *J. Nucl. Mater.* **471** 175–83
- [14] Katoh Y *et al* 2019 Response of unalloyed tungsten to mixed spectrum neutrons *J. Nucl. Mater.* **520** 193–207
- [15] Garrison L, Katoh Y, Snead L L, Byun T S, Reiser J and Rieth M 2016 Irradiation effects in tungsten-copper laminate composite *J. Nucl. Mater.* **481** 134–46
- [16] Garrison L M, Katoh Y and Kiran Kumar N A P 2019 Mechanical properties of single-crystal tungsten irradiated in a mixed spectrum fission reactor *J. Nucl. Mater.* **518** 208–25
- [17] Habainy J, Dai Y, Lee Y and Iyengar S 2019 Mechanical properties of tungsten irradiated with high-energy protons and spallation neutrons *J. Nucl. Mater.* **514** 189–95
- [18] Li M Y and You J H 2015 Interpretation of the deep cracking phenomenon of tungsten monoblock targets observed in high-heat-flux fatigue tests at 20 MW/m<sup>2</sup> *Fusion Eng. Des.* **101** 1–8
- [19] Hirai T *et al* 2016 Use of tungsten material for the ITER divertor *Nucl. Mater. Energy.* **9** 616–22
- [20] Villari R *et al* 2013 Nuclear analysis of the ITER full-tungsten divertor *Fusion Eng. Des.* **88** 2006–10
- [21] Matolich J, Nahm H and Moteff J 1974 Swelling in neutron irradiated tungsten and tungsten-25 rhenium *Scr. Metall.* **8** 837–42
- [22] Stork D *et al* 2014 Developing structural, high-heat flux and plasma facing materials for a near-term DEMO fusion power plant: the EU assessment *J. Nucl. Mater.* **455** 277–91
- [23] Lee F, Matolich J and Moteff J 1976 Swelling in neutron irradiated molybdenum based on dimensional changes *J. Nucl. Mater.* **62** 115–7
- [24] Gludovatz B, Wurster S, Hoffmann A and Pippan R 2010 Fracture toughness of polycrystalline tungsten alloys *Int. J. Refract. Met. Hard Mater.* **28** 674–8
- [25] Wurster S *et al* 2013 Recent progress in R&D on tungsten alloys for divertor structural and plasma facing materials *J. Nucl. Mater.* **442** S181–9
- [26] Yin C, Terentyev D, Pardoën T, Petrov R and Tong Z 2019 Ductile to brittle transition in ITER specification tungsten assessed by combined fracture toughness and bending tests analysis *Mater. Sci. Eng. A* **750** 20–30
- [27] ASTM. E 399-12 2012 *Standard Test Method for Linear-Elastic Plane Strain Fracture Toughness K<sub>IC</sub> of Metallic Materials* (West Conshohocken, PA: ASTM international) (<https://doi.org/10.1520/E0399-12>)
- [28] Pelowitz D *et al* 2011 MCNPX 2.7.0 extensions *Technical Report LA-UR-11-02295* (Los Alamos National Laboratory) (<https://doi.org/10.2172/1058045>)
- [29] Dudarev S L 2015 DPA definition and estimates: IAEA CRP (<https://amdis.iaea.org/CRP/IrradiatedTungsten/RCM2/RCM2Presentation-DudarevDPA-2015-09-10.pdf>)
- [30] Stankovskiy A and Van den Eynde G 2012 Advanced method for calculations of core burn-up, activation of structural materials, and spallation products accumulation in accelerator-driven systems *Sci. Tech. Nuclear Installations* **2012** 545103
- [31] NEA 2017 JEFF-3.3 (<https://oecd-nea.org/dbdata/jeff/jeff33/>)
- [32] Brown D A *et al* 2018 ENDF/B-VIII. 0: the 8th major release of the nuclear reaction data library with CIELO-project cross sections, new standards and thermal scattering data *Nucl. Data Sheets* **148** 1–142
- [33] Konobeyev A Y, Fischer U, Korovin Y A and Simakov S 2017 Evaluation of effective threshold displacement energies and other data required for the calculation of advanced atomic displacement cross-sections *Nucl. Energy Technol.* **3** 169–75
- [34] Norgett M, Robinson M and Torrens I 1975 A proposed method of calculating displacement dose rates *Nucl. Eng. Des.* **33** 50–4
- [35] ASTM. E1921-16 2016 *Standard Test Method for Determination of Reference Temperature, T<sub>0</sub>, for Ferritic Steels in the Transition Range* (West Conshohocken, PA: ASTM International) (<https://doi.org/10.1520/E1921-16>)
- [36] Faleschini M, Kreuzer H, Kiener D and Pippan R 2007 Fracture toughness investigations of tungsten alloys and SPD tungsten alloys *J. Nucl. Mater.* **367** 800–5